Tuning of the Ru^{4+} ground-state orbital population in the $4d^4$ Mott insulator Ca_2RuO_4 achieved by La doping

D. Pincini,[1,2,*] L. S. I. Veiga,[1] C. D. Dashwood,[1] F. Forte,[3,4] M. Cuoco,[3,4] R. S. Perry,[1] P. Bencok,[2] A. T. Boothroyd,[5] and D. F. McMorrow[1]

[1]*London Centre for Nanotechnology and Department of Physics and Astronomy, University College London, Gower Street, London WC1E 6BT, United Kingdom*

[2]*Diamond Light Source Ltd., Harwell Science & Innovation Campus, Didcot, Oxfordshire OX11 0DE, United Kingdom*

[3]*CNR-SPIN, I-84084 Fisciano (SA), Italy*

[4]*Dipartimento di Fisica "E. R. Caianiello," Università di Salerno, I-84084 Fisciano (SA), Italy*

[5]*Clarendon Laboratory, Department of Physics, University of Oxford, Oxford OX1 3PU, United Kingdom*

(Received 26 October 2018; published 11 February 2019)

The ground-state orbital occupancy of the Ru^{4+} ion in $Ca_{2-x}La_xRuO_4$[$x = 0$, 0.05(1), 0.07(1), and 0.12(1)] was investigated by performing x-ray absorption spectroscopy (XAS) in the vicinity of the O K edge as a function of the angle between the incident beam and the surface of the single-crystal samples. A minimal model of the hybridization between the O $2p$ states probed at the K edge and the Ru $4d$ orbitals was used to analyze the XAS data, allowing the ratio of hole occupancies $n_{xy}/n_{yz,zx}$ to be determined as a function of doping and temperature. For the samples displaying a low-temperature insulating ground state ($x \leqslant 0.07$), $n_{xy}/n_{yz,zx}$ is found to increase significantly with increasing doping, with increasing temperature acting to further enhance $n_{xy}/n_{yz,zx}$. For the $x = 0.12$ sample, which has a metallic ground state, the XAS spectra are found to be independent of temperature and not to be describable by the minimal hybridization model, while being qualitatively similar to the spectra displayed by the $x \leqslant 0.07$ samples above their insulating to metallic transitions. To understand the origin of the evolution of the electronic structure of $Ca_{2-x}La_xRuO_4$ across its phase diagram, we have performed theoretical calculations based on a model Hamiltonian, comprising electron-electron correlations, crystal field Δ, and spin-orbit coupling λ, of a Ru-O-Ru cluster, with realistic values used to parametrize the various interactions taken from the literature. Our calculations of the Ru hole occupancy as a function of Δ/λ provide an excellent description of the general trends displayed by the data. In particular they establish that the enhancement of $n_{xy}/n_{yz,zx}$ is driven by significant modifications to the crystal field as the tetragonal distortion of the RuO_6 octahedral changes from compressive to tensile with La doping. We have also used our model to show that the hole occupancy of the O $2p$ and Ru $4d$ orbitals displays the same general trend as a function of Δ/λ, thus validating the minimal hybridization model used to analyze the data. In essence, our results suggest that the predominant mechanism driving the emergence of the low-temperature metallic phase in La-doped Ca_2RuO_4 is the structurally induced redistribution of holes within the t_{2g} orbitals, rather than the injection of free carriers.

DOI: 10.1103/PhysRevB.99.075125

I. INTRODUCTION

Ca_2RuO_4 has attracted considerable attention in recent years as the Mott-insulating analog of the unconventional superconductor Sr_2RuO_4 [1–16]. A well-documented metal to insulator transition (MIT) occurs at $T_{MIT} = 357$ K, concomitant with a first-order structural transition from a high-temperature quasitetragonal phase to a low-temperature orthorhombic one (*Pbca* space group) [1,2,4,17]. Contrary to many Mott insulators, such as La_2CuO_4, the nature of the insulating ground state cannot be accounted for by a simple half-filled single-band scenario where the Mott gap emerges due to a high Coulomb interaction U to bandwidth W ratio. In the case of the 2/3-filled t_{2g} manifold of the Ru^{4+} ion ($4d^4$) in Ca_2RuO_4, the electronic band structure is strongly affected by Hund's and spin-orbit couplings, as well as by the crystal field [6,7,14,15,18].

Angle-resolved photoemission measurements [14] and *ab initio* calculations [6,7] indicated that the Mott-insulating state of Ca_2RuO_4 is triggered by the stabilization of the xy orbitals induced by tetragonal compression of the RuO_6 octahedra in the low-temperature *Pbca* structure [3,16]: in this picture, a Mott gap is opened by Coulomb interactions in the narrower half-filled bands spanned by the yz, zx orbitals (for which $W < U$), with a lower band of xy character. In general, the low-energy multiplet structure of the Ru^{4+} ion is expected to arise from the competition between the tetragonal crystal field Δ and the sizable spin-orbit coupling (SOC) λ of $4d$ electrons [5,10,15,19–22]. The latter acts to weakly reconstruct the xy, yz, and zx orbital configuration, yielding a ground-state wave function of mixed orbital character. Although SOC plays an important role in determining the nature of the low-energy spin and orbital excitations in Ca_2RuO_4, previous studies [14] have suggested that it has only a marginal role in driving

*davide.pincini.14@ucl.ac.uk

the insulating phase of this system. This is because the SOC is not large enough to render a strongly coupled spin-orbit J_{eff} state, as is the case for certain iridates [23]. Moreover, even if it were, due to the d^4 filling of the Ru orbitals, the strong SOC regime would result in a singlet $J_{\text{eff}} = 0$ local ground state, which would not facilitate the opening of a Mott gap.

The coupling between lattice and orbital degrees of freedom was highlighted by recent x-ray near-edge absorption spectroscopy (XANES) studies [5,10,15], which revealed that the ground-state t_{2g} orbital population can be effectively tuned by changing the ratio Δ/λ, analogous to the case of the Ir^{4+} ion in perovskite iridates [24]. The low-energy electronic structure is thus expected to be extremely sensitive to structural distortions acting on the local Ru^{4+} crystalline environment.

Dramatic changes in the insulating ground state, including the appearance of superconductivity, have indeed been achieved by means of epitaxial strain [25], application of hydrostatic pressure to bulk crystals [26,27], and internal chemical pressure [16,17,28,29]. The latter has been mainly realized by substitution of Ca with Sr [28], La [16,17], or Pr [29]. This was found to suppress the MIT and drive the system into a metallic state. In particular, our recent neutron scattering measurements [16] revealed that the different radii of the La^{3+} ($r = 1.22$ Å) and Ca^{2+} ($r = 1.18$ Å) ions [30] cause the compressed RuO_6 octahedra of pure Ca_2RuO_4 to be progressively stretched along the **c** axis for increasing doping levels. This is expected to significantly change the local physics of the Ru^{4+} ion and thus have a sizable impact on the parent compound electronic structure. However, experimental studies on La-doped Ca_2RuO_4 reported to date [16,17,31,32] have not addressed in detail the impact of the structural changes on the low-energy electronic structure.

In this paper we report on an O K-edge XANES investigation of the Ru^{4+} t_{2g} orbital occupancy in $Ca_{2-x}La_xRuO_4$ in both the insulating and metallic regions of the phase diagram (Fig. 1) following an approach similar to the one already used for pure Ca_2RuO_4 [5,10] and Ba_2IrO_4 [33]. The XANES measurements are complemented by theoretical calculations based on a model Hamiltonian for the Ru-O-Ru cluster which includes electron-electron correlations, crystal field, and SOC. In the insulating phase, the hole population of the xy orbitals extracted from the absorption spectra is found to significantly increase as a function of the La concentration. Similar to the case of the parent compound [5], the hole occupancy of the doped samples with insulating ground states also appears to be temperature dependent, with an enhanced xy hole population in the paramagnetic phase compared to the low-temperature antiferromagnetic (AFM) one. On the other hand, both temperature and doping are found to have very little impact in the metallic region. The results of our cluster calculations attribute the changes in the orbital population to the tetragonal crystal-field tuning achieved by either La doping or temperature. In particular, the evolution from compressed to elongated RuO_6 octahedra as a function of increasing La content or temperature [16] is found to cause a transfer of holes from the yz, zx to the xy orbitals, consistent with the XANES measurements.

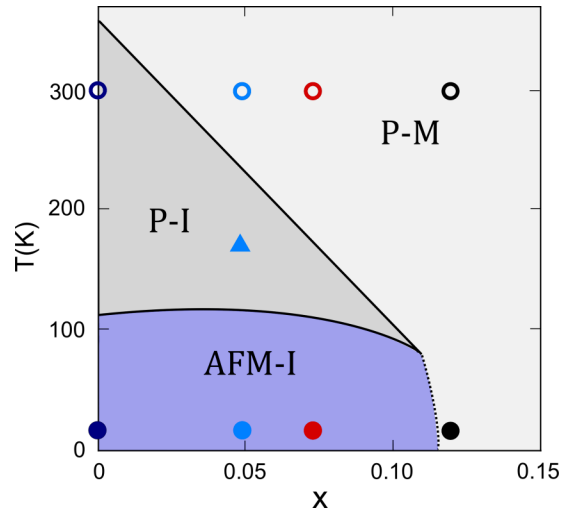

FIG. 1. $Ca_{2-x}La_xRuO_4$ temperature-doping phase diagram showing the paramagnetic metallic (P-M), paramagnetic insulating (P-I), and antiferromagnetic insulating (AFM-I) phases. The solid and open symbols refer to the temperature and La content values in the insulating and metallic regions, respectively, at which the XANES data were collected.

II. EXPERIMENT

A. Samples and methods

Single crystals of $Ca_{2-x}La_xRuO_4$, with $x = 0$, 0.05(1), 0.07(1), and 0.12(1) (corresponding to the nominal dopings $x = 0$, 0.05, 0.10, and 0.15, respectively), were grown through the floating-zone technique as described in Refs. [16,29]. The doping level was determined by means of energy-dispersive x-ray spectroscopy, and the bulk properties were characterized through magnetization and resistivity measurements [16]. The structural properties were also investigated by means of single-crystal neutron diffraction (see Ref. [16] for further details). The parent compound ($x = 0$) MIT is followed upon cooling below $T_N \approx 110$ K by a phase transition to a basal plane canted AFM state [2–4,16,17,31,32,34]. La substitution causes the MIT and Néel temperatures to decrease and be completely suppressed at a doping concentration slightly greater than $x = 0.10$ [16,17]. This is schematically shown in the phase diagram in Fig. 1.

The XANES measurements were performed at the absorption branch of beamline I10 at the Diamond Light Source (Didcot, United Kingdom). Absorption spectra were collected while scanning the incident, circularly polarized x rays ($20 \times 100\ \mu m^2$ spot size) across the O K-edge energy (543.1 eV) for different values of the angle θ between the incident beam and the sample surface normal in the range $0^\circ - 70^\circ$. The degree of circular polarization provided by the APPLE II undulator was always larger than 99% [35]. For each doping level, an equivalent data set was measured at both low ($T = 10$ K) and room temperatures, as indicated by the symbols in Fig. 1. The crystals were mounted on an electrically grounded copper holder and inserted in the UHV sample environment with their crystallographic **c** axis aligned parallel to the incident beam for $\theta = 0^\circ$. The absorption was simultaneously measured in both total-electron yield (TEY) and total-fluorescence yield

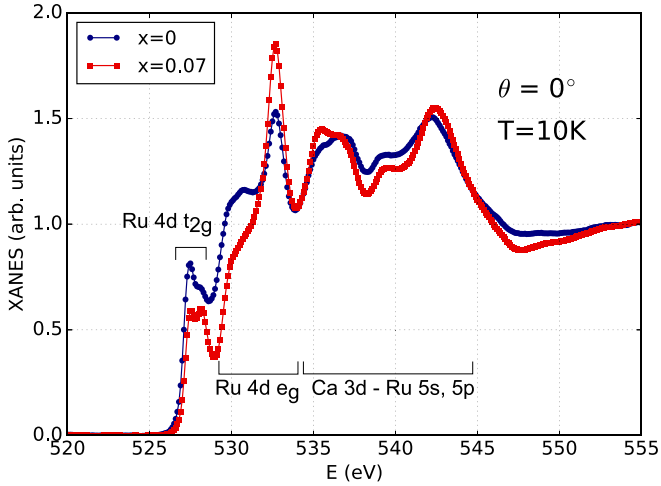

FIG. 2. O K-edge XANES spectra for the parent (blue circles) and $x = 0.07$ (red squares) compounds collected at normal incidence and low temperature. The spectra were normalized using the spectral weight at $E > 553$ eV.

detection modes. The analyses of both sets of data led to similar conclusions, and only the TEY measurements are shown in the present work. Cleaving the crystals *in situ* did not result in any appreciable difference in the absorption spectra with respect to the noncleaved ones, thus excluding any impact of surface contamination.

B. Results

1. Insulating phase

Low-temperature O K-edge spectra at normal incidence for parent Ca_2RuO_4 and the $x = 0.07$ sample are shown in Fig. 2. As first reported by Mizokawa *et al.* [5], the XANES signal shows several features arising from the hybridization of the O $2p$ orbitals with the Ru $4d$ t_{2g} ($E < 530$ eV), Ru $4d$ e_g (530 eV $< E <$ 535 eV), and Ca $3d$/Ru $5s$, $5p$ ($E >$ 535 eV) orbitals. La doping has a significant impact on the relative intensities of the different features, thus revealing the occurrence of sizable changes in the empty density of states of the Ru^{4+} ion. In the present work, we focus our attention on the t_{2g} region of the spectrum, which consists of two separate features centered at around $E \approx 527.5$ eV and $E \approx 528.2$ eV. Following the peak assignments in pure Ca_2RuO_4 [5,10,15] and Sr_2RuO_4 [36,37] and the band structure calculations in Ca_2RuO_4 [38] and Sr_2RuO_4 [39], we attribute the two features to the hybridization of the Ru t_{2g} orbitals with the apical and in-plane O $2p$ orbitals of the RuO_6 octahedra, respectively. Their relative intensity depends on the angle of incidence of the x-ray beam: this is clearly shown in Fig. 3, where spectra collected at low temperature for different θ values in the range $0°-70°$ are reported for the parent compound and $x = 0.07$ crystal. The in-plane/apical intensity ratio tends to increase as θ is increased away from normal incidence. A similar effect also occurs upon doping, as can be seen by comparing spectra collected at the same θ value in the parent and doped samples.

A quantitative analysis of the angular dependence was achieved by fitting the low-energy region of the spectra ($E <$ 530 eV) to the sum of three Gaussian peaks modeling the

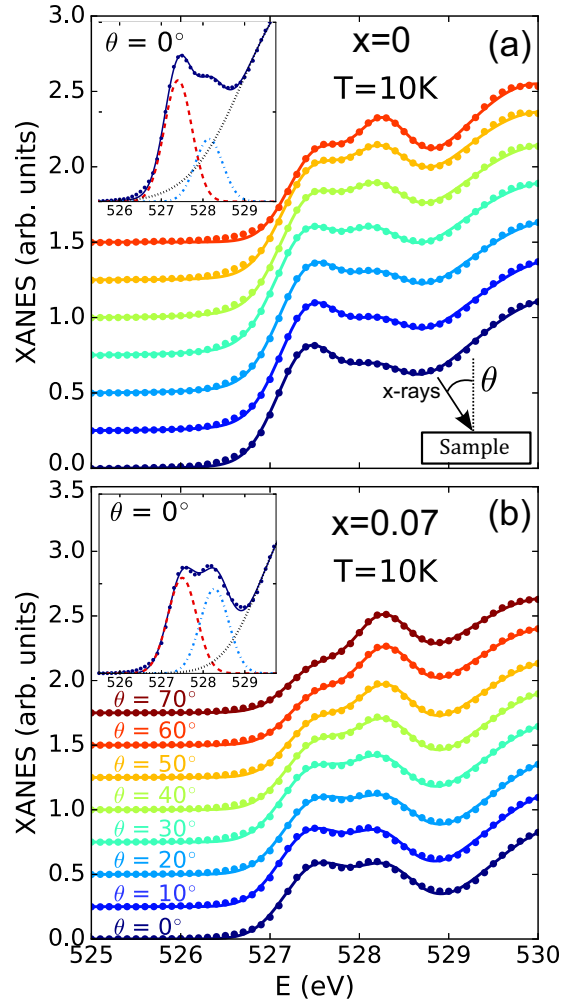

FIG. 3. XANES spectra collected at different values of the angle θ between the incident x-ray beam and the sample surface normal in the (a) parent compound and (b) $x = 0.07$ sample at low temperature. The insets in (a) and (b) show the fit details of the spectra measured at normal incidence ($\theta = 0°$). The measured absorption (solid circles) was fitted to the sum (solid line) of three Gaussian profiles modeling the apical (red dashed line) and in-plane (blue dot-dashed line) O $2p$-Ru t_{2g} features and the e_g region of the spectrum (black dotted line). The corresponding angular dependence of the ratio of in-plane to apical intensities is reported in Fig. 4. Spectra at different angles were normalized using the spectral weight at $E > 553$ eV.

apical and in-plane O $2p$-Ru t_{2g} features and the e_g region of the spectrum at higher energy (see insets in Fig. 3). The results of the fits for the different insulating samples at low temperature are reported in Fig. 4. A clear evolution of the angular dependence is seen as a function of doping, with the in-plane/apical intensity ratio increasing with the La content.

The dependence of the intensity ratio on the incident angle is determined by the dipole matrix elements of the O $1s \rightarrow 2p$ transition. Following the minimal hybridization model already exploited for Ca_2RuO_4 [5,10], the θ dependence of transitions to the O $2p_x$, $2p_y$, and $2p_z$ orbitals for circularly polarized light [41] is given by $\frac{1}{2}\cos^2\theta$, $\frac{1}{2}$, and $\frac{1}{2}\sin^2\theta$, respectively [5,33]. The $2p_{x,y}$ and $2p_z$ orbitals of the in-plane O atoms hybridize with the Ru xy and yz, zx orbitals, respectively.

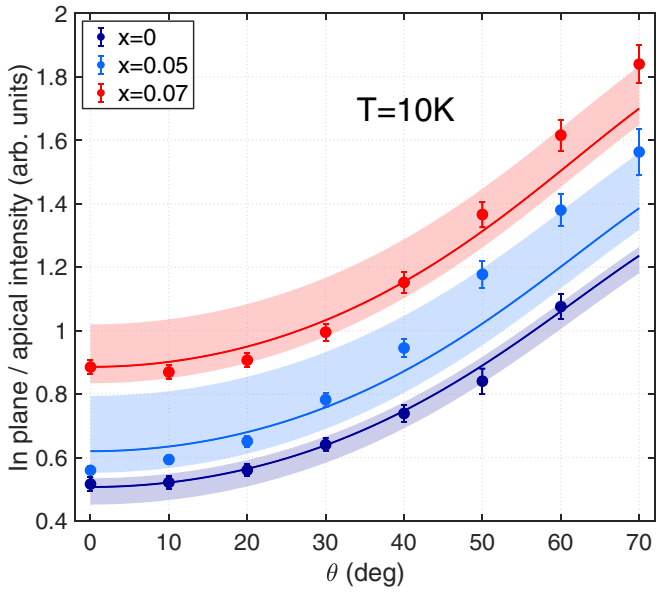

FIG. 4. Ratio of the intensities of the in-plane to apical O $2p$-Ru t_{2g} features of the XANES spectra in the parent (dark blue circles), $x = 0.05$ (light blue circles), and $x = 0.07$ (red circles) compounds at low temperature. The solid symbols were extracted through a fit of the measured XANES spectra analogous to the ones shown in Fig. 3 (see the Supplemental Material [40] for the XANES spectra of the $x = 0.05$ sample), while the solid lines correspond to the best fit to the cross sections of Eq. (2), and the shaded areas correspond to estimated confidence intervals in these fits. The resulting $n_{xy}/n_{yz,zx}$ ratios are reported in Fig. 5.

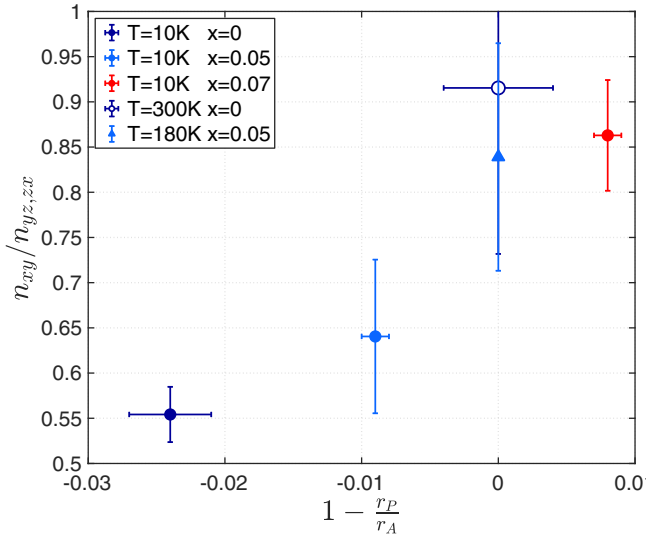

FIG. 5. Hole occupancy ratio $n_{xy}/n_{yz,zx}$ at different temperatures as a function of tetragonality $1 - (r_P/r_A)$, extracted from the angular dependence of the ratio of the in-plane to apical O $2p$-Ru t_{2g} intensities in the XANES spectra in the insulating region of the phase diagram (see Fig. 4 for the $T = 10$ K data set and the Supplemental Material [40] for the measurements at higher temperature). The bond lengths $r_{A,P}$ were obtained from Ref. [16] for all doping and temperature combinations, except $x = 0.05$, $T = 180$ K, for which it was assumed $r_A = r_P$. The symbols follow the same convention used in Fig. 1. The vertical error bars correspond to the estimated confidence intervals shown in Fig. 4, while the horizontal error bars correspond to the uncertainties in the bond lengths [16].

On the other hand, the $2p_x$ ($2p_y$) orbital of the apical O atoms hybridizes with the Ru zx (yz) orbital. The XANES intensities of the apical (I_A) and in-plane (I_P) oxygen features are thus given by the following relations [5]:

$$I_A(\theta) \propto r_A^{-3.5}\frac{1}{2}(\cos^2\theta + 1)n_{yz,zx},$$
$$I_P(\theta) \propto r_P^{-3.5}\left[\frac{1}{2}(\cos^2\theta + 1)n_{xy} + \frac{1}{2}\sin^2\theta\, n_{yz,zx}\right], \quad (1)$$

giving the ratio

$$\frac{I_P}{I_A} \propto \left(\frac{r_A}{r_P}\right)^{3.5}\left[\frac{n_{xy}}{n_{yz,zx}} + \frac{\sin^2\theta}{\cos^2\theta + 1}\right], \quad (2)$$

where r_A (r_P) is the apical (in-plane) Ru-O bond length and n_{xy} ($n_{yz,zx} = n_{yz} + n_{zx}$) is the number of holes in the Ru xy ($yz + zx$) orbitals. In Eq. (1), we assumed that the hybridization strength decays with the Ru-O bond length as $r^{-3.5}$, similar to a previous XANES investigation on the parent compound [10]. In addition, the cross sections of Eq. (1) do not depend on the particular in-plane orientation of the crystallographic **a** and **b** axes, which was not defined in our measurements.

It should be noted that determining the Ru $4d$ orbital occupancy through the direct measurement of the oxygen $2p$ orbitals is not *a priori* obvious since one needs to understand the correspondence between the hole distribution in the two orbitals. However, as will be discussed later, our theoretical calculations indicate that the hole occupancy of the O $2p$ and Ru $4d$ orbitals show the same general trend, which validates the minimal hybridization model used to analyze the data.

Equation (2) was used to fit the measured angular dependences and extract the hole occupancy ratio $n_{xy}/n_{yz,zx}$ (note that the arbitrary scale factor which relates the cross sections to the intensity derived from the XANES spectra means that only the ratio is accessible through a fit of the data rather than the separate quantities n_{xy} and $n_{yz,zx}$). The best-fit curves for the insulating samples at low temperature are plotted as solid lines in Fig. 4, with estimated confidence intervals in the fits represented by shaded areas. These fits were obtained considering $r_A = 1.971$, 1.987, 2.007 Å and $r_P = 2.017$, 2.005, 1.990 Å for $x = 0$, 0.05, 0.07, respectively [16]. An angular offset was also included as a free fitting parameter to account for small misalignments of the sample surface normal with respect to the incident x-ray direction. Equation (2) provides a good description of the trends in the experimental data: the resulting $n_{xy}/n_{yz,zx}$ values are reported in Fig. 5 as a function of the tetragonality $1 - (r_P/r_A)$. Here, the values extracted from the XANES spectra measured in the parent compound at room temperature and the $x = 0.05$ sample in the paramagnetic-insulating (P-I) phase ($T = 180$ K) are also shown. Given the lack of detailed structural information at $T = 180$ K, we set $r_A = r_P$ at this temperature.

Our measurements indicate that, at low temperature, the $n_{xy}/n_{yz,zx}$ value increases from 0.55(3) in the parent compound up to 0.86(6) in the $x = 0.07$ sample. Consistent with an early

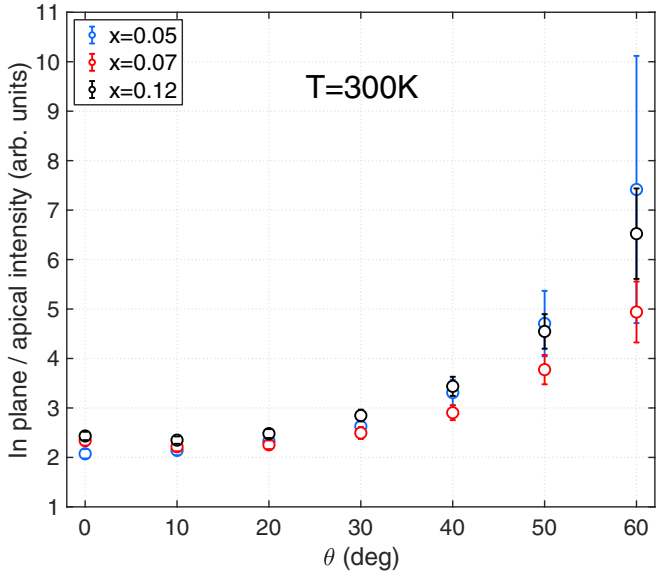

FIG. 6. Ratio of the intensities of the in-plane to apical O $2p$-Ru t_{2g} features of the XANES spectra in the $x = 0.05$ (blue circles), $x = 0.07$ (red circles), and $x = 0.12$ (black circles) samples at room temperature. The symbols were extracted through a fit of the measured XANES spectra analogous to Fig. 4 (see the Supplemental Material [40] for the corresponding spectra).

report on pure Ca_2RuO_4 [5], the hole occupancy of the xy orbitals is also found to increase up to $n_{xy}/n_{yz,zx} \approx 1$ upon warming to the P-I phase in the $x = 0$ ($T = 300$ K) and $x = 0.05$ ($T = 180$ K) samples. Previous XANES studies on the parent compound reported somewhat smaller $n_{xy}/n_{yz,zx}$ values in the AFM phase [5,10]. In particular, Mizokawa *et al.* [5] found $n_{xy}/n_{yz,zx} \approx 0.3$ using circularly polarized light at $T = 90$ K, while XANES measurements performed with linearly polarized x rays in normal and grazing incidence geometries at $T = 20$ K reported a value $0.15 < n_{xy}/n_{yz,zx} < 0.2$ [10]. A significant change in the orbital population between 90 and 20 K seems unlikely given the substantial insensitivity of the Ca_2RuO_4 crystal structure to the temperature below the Néel transition [3]. The variability between different studies might stem from small variations in the oxygen content: these are likely to affect the orbital population at the Ru site due to the covalent character of the Ru-O bond [3]. Although the origin of the discrepancy remains an open issue, this does not affect the validity of our conclusions.

2. *Metallic phase*

The in-plane and apical features of the XANES spectra exhibit a markedly different behavior in the metallic phase (see Fig. 1). In particular, the apical feature is found to be less pronounced than the in-plane one at all θ values. Figure 6 shows the angular dependence measured in the doped crystals at room temperature (see the Supplemental Material [40] for the corresponding XANES spectra). In contrast to the insulating phase, the doping concentration does not significantly affect the angular dependence of the XANES features. The same is true for temperature, as shown in the low-temperature data collected in the $x = 0.12$ sample [40]. Equation (2) does not provide a satisfactory fit of the data in this case. This is not surprising since the simple hybridization model is based on an atomic orbital picture and cannot properly account for the itinerant character of the Ru $4d$ electrons in the metallic state.

III. THEORETICAL CALCULATIONS

The recent report of tetragonal field tuning achieved by La substitution [16] points towards a structural origin for the changes in the hole occupancy extracted from the XANES data. Following this reasoning, we investigated the evolution of the orbital-dependent hole occupancy of the Ru $4d$ and O $2p$ electronic states as a function of the ratio Δ/λ of the tetragonal crystal field Δ and SOC constant λ. Ca_2RuO_4 is a spin-orbit coupled Mott insulator with strong sensitivity to structural changes [16,17,25–29]. Therefore, it is of primary importance to include in the modeling all the relevant microscopic ingredients, i.e., the atomic Coulomb interaction, the SOC, the p-d charge transfer processes, and the octahedral distortions. Moreover, since the XANES measurements of Sec. II give direct insight into the oxygen $2p$ states, one relevant issue here is to assess how the Ru $4d$ orbital occupation is related to O $2p$ one. Since both the SOC and the octahedral rotations mix the orbital degrees of freedom, it is not *a priori* obvious to deduce how the changes in the hole distribution in the $4d$ orbitals are related to the ones in the $2p$ states at the oxygen site.

The calculations were performed by solving a model Hamiltonian for the Ru-O-Ru cluster that is able to capture the main electronic processes impacting the $4d$ and $2p$ orbital occupations in the AFM insulating phase of $Ca_{2-x}La_xRuO_4$. An analogous approach was recently successfully used to interpret the spectrum of Ru^{4+} electronic excitations probed by means of resonant inelastic x-ray scattering (RIXS) at the O K edge [15]. The model Hamiltonian for the relevant bands close to the Fermi level for the electrons within the ruthenium-oxygen plane is based on the interaction terms at the Ru and O sites and the charge transfer processes for the Ru-O electronic connectivity. The local ruthenium Hamiltonian $H_{\rm loc}$ [42,43] includes the complete Coulomb interaction for the t_{2g} electrons, the SOC, and the tetragonal crystal-field potential. The various terms are generally expressed by

$$
\begin{aligned}
H_{\text{el-el}}(i) &= U \sum n_{i\alpha\uparrow} n_{i\alpha\downarrow} - 2J_{\rm H} \sum_{\alpha<\beta} \mathbf{S}_{i\alpha} \cdot \mathbf{S}_{i\beta} \\
&\quad + \left(U - \frac{5J_{\rm H}}{2}\right) \sum_{\alpha<\beta} n_{i\alpha} n_{i\beta} \\
&\quad + J_H \sum_{\alpha<\beta} d^{\dagger}_{i\alpha\uparrow} d^{\dagger}_{i\alpha\downarrow} d_{i\beta\uparrow} d_{i\beta\downarrow}, \\
H_{\rm SOC}(i) &= \lambda \sum_{\alpha,\sigma} \sum_{\beta,\sigma'} d^{\dagger}_{i\alpha\sigma} (\mathbf{l}_{\alpha\beta} \cdot \mathbf{s}_{\sigma\sigma'}) d_{i\beta\sigma'}, \\
H_{\rm cf}(i) &= \varepsilon_{xy} n_{i,xy} + \varepsilon_z (n_{i,xz} + n_{i,yz}), \\
H_{\rm loc}(i) &= H_{\text{el-el}}(i) + H_{\rm SOC}(i) + H_{\rm cf}(i),
\end{aligned}
\tag{3}
$$

where i labels the site; α and β are indices running over the three orbitals in the t_{2g} sector, i.e., $\alpha, \beta \in \{d_{xy}, d_{xz}, d_{yz}\}$; and $d^{\dagger}_{i\alpha\sigma}$ is the creation operator of an electron with spin σ at site i in orbital α. The interaction is parametrized by the intraorbital Coulomb interaction U and the Hund's coupling J_{H}. The strength of the tetragonal distortions is expressed by the amplitude Δ, with $\Delta = (\varepsilon_{xy} - \varepsilon_z)$. A negative (positive) Δ corresponds to a flat (elongated) octahedral configuration with a tendency to different orbital occupations in the two regimes.

Furthermore, we consider the ruthenium-oxygen hopping, which includes all the symmetry-allowed terms according to the Slater-Koster rules [44,45] for a given bond connecting a ruthenium atom to an oxygen atom along a given symmetry direction. Here, we allow for a rotation of the octahedra around the **c** axis assuming that the planar Ru-O-Ru bond can form a generic angle $\beta = (180^{\circ} - \phi)$. The case with $\phi = 0$ corresponds to the tetragonal undistorted bond, while a nonvanishing value of ϕ arises when the RuO_6 octahedra are rotated around the **c** axis. A value of $\phi = 15^{\circ}$ was considered in the present analysis, which is in the range of the experimentally observed octahedral rotation for Ca_2RuO_4 [16].

Concerning the employed electronic parameters, we took as a reference those previously used for Ca_2RuO_4. In the latter, the octahedra become flat below the structural transition [3,16]: Δ is thus negative, and according to first-principles calculations or estimates employed to reproduce the RIXS [15] or inelastic neutron scattering [11] spectra and magnetic anisotropy of the antiferromagnetic phase [46], its magnitude is $\sim$200$-$300 meV. The material-specific values $\lambda =$ 0.075 eV, $U = 2$ eV, and J_H in the range 0.35–0.5 eV [5,47] were also considered. Similar values for Δ, U, and J_H were used for band structure calculations for Ca_2RuO_4 [14], while a ratio $|\Delta|/\lambda$ in the range of $\sim$3$-$4 was found to correctly reproduce the spin excitations observed by inelastic neutron scattering [11]. For the hopping amplitudes, we considered a representative set of electronic parameters for the Ru-O-Ru cluster that is consistent with typical amplitudes obtained from first-principles calculations for ruthenium oxides [7,15,38,48–50]. Given the limited impact of La substitution on the Ru-O-Ru bond angle and octahedral tilt away from the **c** axis [16], we assumed that the hopping amplitudes are not quantitatively affected by the La concentration.

The evolution of the Ru xy, yz, and zx orbital population can be conveniently described in terms of the expectation values n_α of the hole occupancy operators $\tilde{n}_\alpha$ ($\alpha = xy, yz, zx$). These are reported in Fig. 7(a) as a function of Δ/λ. Here, a value $n_{xy}/n_{yz,zx} = 0.5$ for the ratio of the xy and $yz + zx$ hole occupancies corresponds to an equal population of holes in each of the xy, yz, and zx states. As expected, a transfer of holes from the yz, zx to the xy orbitals takes place in going from flat ($\Delta < 0$) to elongated ($\Delta > 0$) RuO_6 octahedra. In particular, we observe that the crossover from $n_{xy}/n_{yz,zx} < 0.5$ to $n_{xy}/n_{yz,zx} > 0.5$ starts already in the regime of flat octahedra ($\Delta/\lambda \sim -1$), after which the system evolves rapidly to a configuration with an equal number of holes in the xy and $yz + zx$ orbitals. The latter corresponds to $n_{xy}/n_{yz,zx} = 1$ and is almost completely realized already for $\Delta = 0$. We find that such behavior is quite robust and weakly depends on the amplitude of the Coulomb interaction. More specifically, a variation of the local atomic correlations leads to a shift of the onset of the hole transfer from the xy to the yz, zx orbitals in the direction of octahedral compression.

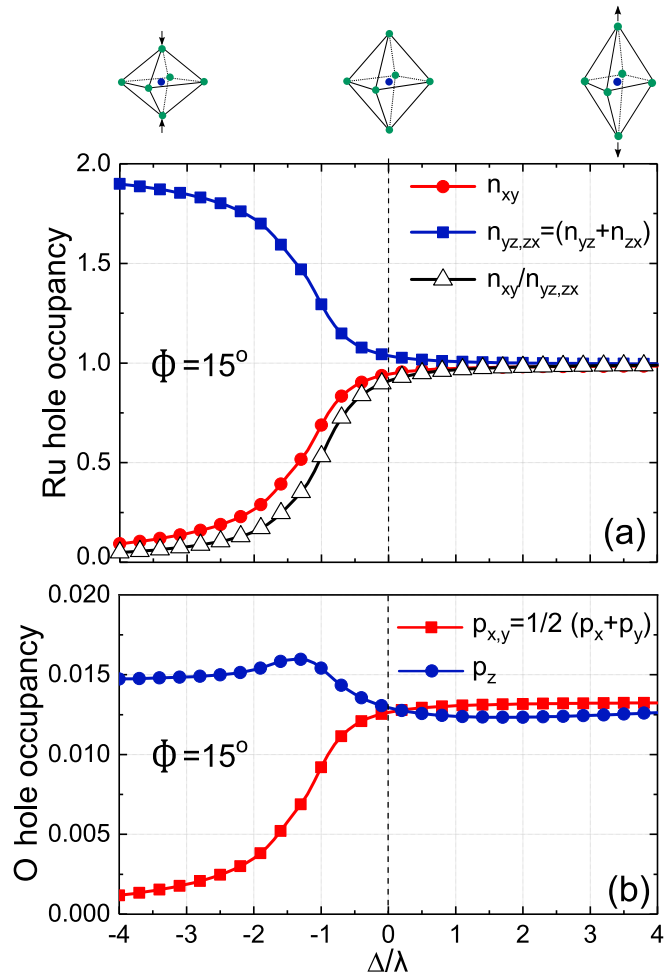

FIG. 7. Calculated hole occupancy of the (a) Ru t_{2g} and (b) O $2p$ orbitals as a function of the ratio Δ/λ between the tetragonal crystal-field potential and the SOC. The calculations were performed considering the ground state of the Ru-O-Ru cluster with $J_H =$ 0.4 eV, $U = 2.2$ eV, and $\phi = 15^{\circ}$, where ϕ is the RuO_6 octahedra in-plane rotation. The diagram at the top schematically illustrates the tetragonal distortion of the RuO_6 octahedra for the different values of Δ/λ.

Another interesting aspect emerging from our calculations concerns the correspondence between the hole distribution in the $2p$ orbitals at the oxygen site and that of the Ru $4d$ states. Our results show that the number of holes in the planar $p_{x,y}$ (p_z) orbitals exhibits the same trend of the xy (yz, zx) states as a function of the tetragonal distortions [Fig. 7(b)]. This is particularly relevant as it justifies the possibility of extracting the evolution of the hole distribution in the Ru bands from the spectroscopic analysis performed at the O sites by means of Eq. (2).

IV. DISCUSSION

The results of the cluster calculations presented in Sec. III clearly identify the tetragonal crystal-field tuning induced by

La substitution (or temperature) that we have recently reported [16] as the main cause of the orbital hole occupancy evolution extracted from the XANES measurements in the insulating phase. In particular, the neutron scattering investigation of Ref. [16] revealed that the internal chemical pressure caused by La doping results in a progressive elongation of the RuO_6 octahedra along the apical Ru-O direction. They are compressed by about -2.4% in the parent compound [3,16]. The compression reduces to -0.9% in the $x = 0.05$ sample, while the octahedra are elongated by about 0.8% for $x = 0.07$ [16]. Temperature was found to have a similar effect in the parent compound insulating phase: the tetragonal distortion is released upon warming, leading to almost regular octahedra at $T = 300$ K [3,16].

Consistent with the calculations displayed in Fig. 7(a), the ratio $n_{xy}/n_{yz,zx}$ increases in going from the parent to the doped compounds and is larger in the P-I phase than in the AFM one. In particular, the xy hole population at low temperature is significantly enhanced in the case of the $x = 0.07$ elongated octahedra with respect to the $x = 0$, 0.05 compressed ones. The attribution of the observed evolution to structural effects is further confirmed by the insensitivity of the XANES spectra of the metallic samples to both temperature and La content. Our recent neutron diffraction study [16] indeed found that the RuO_6 octahedra are elongated by about 4.3%–4.5% in the metallic region of the phase diagram regardless of the temperature or doping level.

The results presented in Fig. 7 also contain important information with relevance to the impact of the spin-orbit coupling on the Ru 4d orbital occupancy. It explicitly demonstrates how the orbital population of the Ru t_{2g} states are tuned by the tetragonal crystal-field potential in the presence of SOC and Coulomb interactions, providing direct insight into the energy scales expressing the competition between these parameters. Moreover, the faster transfer of holes from the zx, yz to the xy orbitals already in the regime of flat octahedra ($\Delta/\lambda \sim -1$) is a direct consequence of SOC as it allows the mixing of these orbitals. In this case, SOC acts to weaken the effect of the crystal-field potential. The emptying out of the xy orbital, then, leads to a breakdown of the Mott-insulating state and the formation of a metallic state which is electronically similar to the high-temperature phase of Ca_2RuO_4, where it has elongated octahedra.

Despite the structural modifications induced by La doping unveiled by neutron diffraction [16], the corresponding effect on the Ru^{4+} electronic structure is not *a priori* obvious. Indeed, La substitution can also introduce free carriers at the Ru sites. In this case, one would observe a decrease in the hole occupation of yz, zx states without significant modifications in the xy hole density. Such behavior would thus result in an increase in the $n_{xy}/n_{yz,zx}$ ratio upon doping, similar to what is expected when considering structural effects alone (Fig. 7). However, recent investigations of La-doped [16] and Pr-doped [29] Ca_2RuO_4 strongly suggest that, in contrast to lightly doped cuprates [51] and iridates [52,53], the doped electrons remain fully localized in the low-temperature insulating phase, confirming the predominance of the structural effects on the ground-state orbital occupancy of the Ru^{4+} ion.

The ground-state properties of the Ru^{4+} ion in Ca_2RuO_4 were previously described in terms of a minimal Hamiltonian including tetragonal crystal field and SOC, which was used to account for the electronic excitation spectrum probed by O K-edge RIXS [10]. The model in Ref. [10] represents an oversimplification of the electronic properties of Ca_2RuO_4 as, in contrast to the cluster calculations of Sec. III, it neglects many-body effects of the system of four Ru^{4+} t_{2g} electrons and the interaction with the ligand oxygens. Nonetheless, this minimal Hamiltonian also predicts an enhancement of the xy hole populations in going from octahedral compression to octahedral elongation [40], in qualitative agreement with our results

Although the trends seen in our data qualitatively follow the predictions of the model (Sec. III), the measured absolute values of $n_{xy}/n_{yz,zx}$ are only in partial agreement with the calculated ones. This is mainly due to the fact that the $n_{xy}/n_{yz,zx}$ values derived through the minimal hybridization model of Eq. (2) are only approximate and do not allow a precise quantitative estimation. Despite the quantitative discrepancies, the trend confirmed by the calculations highlights the sensitivity of the spin-orbit entangled ground state of the Ru^{4+} ion to structural distortions.

V. CONCLUDING REMARKS

In conclusion, our XANES investigation has revealed that the elongation of the RuO_6 octahedra induced by either La substitution or temperature increase results in an enhancement of the xy hole population of the Ru^{4+} ground-state wave function in the insulating region of the temperature-doping phase diagram. On the other hand, the hole occupancy shows little variation with temperature and doping in the metallic phase, consistent with the lack of significant structural changes. The sensitivity of the orbital population of the Ru^{4+} ground state to the local crystalline environment has been shown to directly result from the peculiar entanglement of xy, yz, and zx orbitals caused by the interplay of electronic correlations, crystal field, and SOC of 4d electrons. Our findings confirm the subtle nature of the low-energy Hamiltonian of perovskite ruthenates, where, despite the presence of a rather weaker spin-orbit interaction compared to the case of iridium oxides, a peculiar coupling between orbital and lattice degrees of freedom still arises from the competition between tetragonal field and SOC. Moreover, the results highlight the unique impact of La substitution on the Mott-band-insulating state of Ca_2RuO_4, where the low-temperature metallic phase is stabilized by the structurally induced redistribution of holes in the t_{2g} orbitals rather than by the injection of electrons.

ACKNOWLEDGMENTS

The authors would like to thank S. Riccò for her great help during the sample growth and characterization and J. Chang, S. Riccò, F. Baumberger, M. M. Sala, M. Rossi, and S. Boseggia for helpful discussions. This work is supported by the UK Engineering and Physical Sciences Research Council (Grants No. EP/N027671/1, No. EP/N034694/1, and No. EP/N034872/1).

[1] G. Cao, S. McCall, M. Shepard, J. E. Crow, and R. P. Guertin, Phys. Rev. B **56**, R2916 (1997).

[2] S. Nakatsuji, S.-i. Ikeda, and Y. Maeno, J. Phys. Soc. Jpn. **66**, 1868 (1997).

[3] M. Braden, G. André, S. Nakatsuji, and Y. Maeno, Phys. Rev. B **58**, 847 (1998).

[4] C. S. Alexander, G. Cao, V. Dobrosavljevic, S. McCall, J. E. Crow, E. Lochner, and R. P. Guertin, Phys. Rev. B **60**, R8422 (1999).

[5] T. Mizokawa, L. H. Tjeng, G. A. Sawatzky, G. Ghiringhelli, O. Tjernberg, N. B. Brookes, H. Fukazawa, S. Nakatsuji, and Y. Maeno, Phys. Rev. Lett. **87**, 077202 (2001).

[6] A. Liebsch and H. Ishida, Phys. Rev. Lett. **98**, 216403 (2007).

[7] E. Gorelov, M. Karolak, T. O. Wehling, F. Lechermann, A. I. Lichtenstein, and E. Pavarini, Phys. Rev. Lett. **104**, 226401 (2010).

[8] I. Zegkinoglou, J. Strempfer, C. S. Nelson, J. P. Hill, J. Chakhalian, C. Bernhard, J. C. Lang, G. Srajer, H. Fukazawa, S. Nakatsuji, Y. Maeno, and B. Keimer, Phys. Rev. Lett. **95**, 136401 (2005).

[9] G. Khaliullin, Phys. Rev. Lett. **111**, 197201 (2013).

[10] C. G. Fatuzzo, M. Dantz, S. Fatale, P. Olalde-Velasco, N. E. Shaik, B. Dalla Piazza, S. Toth, J. Pelliciari, R. Fittipaldi, A. Vecchione, N. Kikugawa, J. S. Brooks, H. M. Rønnow, M. Grioni, C. Rüegg, T. Schmitt, and J. Chang, Phys. Rev. B **91**, 155104 (2015).

[11] A. Jain, M. Krautloher, J. Porras, G. H. Ryu, D. P. Chen, D. L. Abernathy, J. T. Park, A. Ivanov, J. Chaloupka, G. Khaliullin, B. Keimer, and B. J. Kim, Nat. Phys. **13**, 633 (2017).

[12] S. Kunkemöller, D. Khomskii, P. Steffens, A. Piovano, A. A. Nugroho, and M. Braden, Phys. Rev. Lett. **115**, 247201 (2015).

[13] S. Kunkemöller, E. Komleva, S. V. Streltsov, S. Hoffmann, D. I. Khomskii, P. Steffens, Y. Sidis, K. Schmalzl, and M. Braden, Phys. Rev. B **95**, 214408 (2017).

[14] D. Sutter, C. G. Fatuzzo, S. Moser, M. Kim, R. Fittipaldi, A. Vecchione, V. Granata, Y. Sassa, F. Cossalter, G. Gatti, M. Grioni, H. M. Rønnow, N. C. Plumb, C. E. Matt, M. Shi, M. Hoesch, T. K. Kim, T. R. Chang, H. T. Jeng, C. Jozwiak, A. Bostwick, E. Rotenberg, A. Georges, T. Neupert, and J. Chang, Nat. Commun. **8**, 15176 (2017).

[15] L. Das, F. Forte, R. Fittipaldi, C. G. Fatuzzo, V. Granata, O. Ivashko, M. Horio, F. Schindler, M. Dantz, Y. Tseng, D. E. McNally, H. M. Rønnow, W. Wan, N. B. Christensen, J. Pelliciari, P. Olalde-Velasco, N. Kikugawa, T. Neupert, A. Vecchione, T. Schmitt, M. Cuoco, and J. Chang, Phys. Rev. X **8**, 011048 (2018).

[16] D. Pincini, S. Boseggia, R. Perry, M. J. Gutmann, S. Riccò, L. S. I. Veiga, C. D. Dashwood, S. P. Collins, G. Nisbet, A. Bombardi, D. G. Porter, F. Baumberger, A. T. Boothroyd, and D. F. McMorrow, Phys. Rev. B **98**, 014429 (2018).

[17] H. Fukazawa and Y. Maeno, J. Phys. Soc. Jpn. **70**, 460 (2001).

[18] A. Georges, L. de' Medici, and J. Mravlje, Ann. Rev. Cond. Mat. Phys. **4**, 137 (2013).

[19] S. Nakatsuji and Y. Maeno, Phys. Rev. B **62**, 6458 (2000).

[20] G. Q. Liu, Phys. Rev. B **84**, 235136 (2011).

[21] G. Q. Liu, Phys. Rev. B **88**, 104428 (2013).

[22] M. Kurokawa and T. Mizokawa, Phys. Rev. B **66**, 024434 (2002).

[23] B. J. Kim, H. Jin, S. J. Moon, J.-Y. Kim, B.-G. Park, C. S. Leem, J. Yu, T. W. Noh, C. Kim, S.-J. Oh, J. H. Park, V. Durairaj, G. Cao, and E. Rotenberg, Phys. Rev. Lett. **101**, 076402 (2008).

[24] M. Moretti Sala, S. Boseggia, D. F. McMorrow, and G. Monaco, Phys. Rev. Lett. **112**, 026403 (2014).

[25] H. Nobukane, K. Yanagihara, Y. Kunisada, Y. Ogasawara, K. Nomura, Y. Asano, and S. Tanda, arXiv:1703.09459.

[26] P. L. Alireza, F. Nakamura, S. K. Goh, Y. Maeno, S. Nakatsuji, Y. T. C. Ko, M. Sutherland, S. Julian, and G. G. Lonzarich, J. Phys. Condens. Matter **22**, 052202 (2010).

[27] P. Steffens, O. Friedt, P. Alireza, W. G. Marshall, W. Schmidt, F. Nakamura, S. Nakatsuji, Y. Maeno, R. Lengsdorf, M. M. Abd-Elmeguid, and M. Braden, Phys. Rev. B **72**, 094104 (2005).

[28] O. Friedt, M. Braden, G. André, P. Adelmann, S. Nakatsuji, and Y. Maeno, Phys. Rev. B **63**, 174432 (2001).

[29] S. Riccò, M. Kim, A. Tamai, S. M. Walker, F. Y. Bruno, I. Cucchi, E. Cappelli, C. Besnard, T. K. Kim, P. Dudin, M. Hoesch, M. Gutmann, A. Georges, R. S. Perry, and F. Baumberger, Nat. Commun. **9**, 4535 (2018).

[30] R. D. Shannon, Acta Crystallogr., Sect. A **32**, 751 (1976).

[31] G. Cao, C. S. Alexander, S. McCall, J. E. Crow, and R. P. Guertin, J. Magn. Magn. Mater. **226–230**, 235 (2001).

[32] G. Cao, S. McCall, V. Dobrosavljevic, C. S. Alexander, J. E. Crow, and R. P. Guertin, Phys. Rev. B **61**, R5053 (2000).

[33] M. M. Sala, M. Rossi, S. Boseggia, J. Akimitsu, N. B. Brookes, M. Isobe, M. Minola, H. Okabe, H. M. Rønnow, L. Simonelli, D. F. McMorrow, and G. Monaco, Phys. Rev. B **89**, 121101 (2014).

[34] H. Fukazawa, S. Nakatsuji, and Y. Maeno, Physica B (Amsterdam, Neth.) **281–282**, 613 (2000).

[35] H. Wang, P. Bencok, P. Steadman, E. Longhi, J. Zhu, and Z. Wang, J. Synchrotron Radiat. **19**, 944 (2012).

[36] M. Schmidt, T. R. Cummins, M. Bürk, D. H. Lu, N. Nücker, S. Schuppler, and F. Lichtenberg, Phys. Rev. B **53**, R14761 (1996).

[37] S. J. Moon, M. W. Kim, K. W. Kim, Y. S. Lee, J.-Y. Kim, J.-H. Park, B. J. Kim, S.-J. Oh, S. Nakatsuji, Y. Maeno, I. Nagai, S. I. Ikeda, G. Cao, and T. W. Noh, Phys. Rev. B **74**, 113104 (2006).

[38] Z. Fang, N. Nagaosa, and K. Terakura, Phys. Rev. B **69**, 045116 (2004).

[39] D. J. Singh, Phys. Rev. B **52**, 1358 (1995).

[40] See Supplemental Material at http://link.aps.org/supplemental/10.1103/PhysRevB.99.075125 for additional data and further details on the data analysis.

[41] Here, we consider the representative case where the crystallographic [010] direction lies along the θ rotation axis for the expression of the angular dependence of the transitions to the $2p$ orbitals. The resulting angular dependence of the intensity of the XANES features does not depend on this assumption.

[42] M. Cuoco, F. Forte, and C. Noce, Phys. Rev. B **74**, 195124 (2006).

[43] M. Cuoco, F. Forte, and C. Noce, Phys. Rev. B **73**, 094428 (2006).

[44] W. A. Harrison, *Electronic Structure and the Properties of Solids: The Physics of the Chemical Bond* (Dover Publications, INC., New York, 2012).

[45] W. Brzezicki, C. Noce, A. Romano, and M. Cuoco, Phys. Rev. Lett. **114**, 247002 (2015).

[46] D. G. Porter, V. Granata, F. Forte, S. Di Matteo, M. Cuoco, R. Fittipaldi, A. Vecchione, and A. Bombardi, Phys. Rev. B **98**, 125142 (2018).

[47] C. N. Veenstra, Z. H. Zhu, M. Raichle, B. M. Ludbrook, A. Nicolaou, B. Slomski, G. Landolt, S. Kittaka, Y. Maeno, J. H. Dil, I. S. Elfimov, M. W. Haverkort, and A. Damascelli, Phys. Rev. Lett. **112**, 127002 (2014).

[48] M. Malvestuto, V. Capogrosso, E. Carleschi, L. Galli, E. Gorelov, E. Pavarini, R. Fittipaldi, F. Forte, M. Cuoco, A. Vecchione, and F. Parmigiani, Phys. Rev. B **88**, 195143 (2013).

[49] V. Granata, L. Capogna, F. Forte, M.-B. Lepetit, R. Fittipaldi, A. Stunault, M. Cuoco, and A. Vecchione, Phys. Rev. B **93**, 115128 (2016).

[50] F. Forte, M. Cuoco, and C. Noce, Phys. Rev. B **82**, 155104 (2010).

[51] A. Damascelli, Z. Hussain, and Z.-X. Shen, Rev. Mod. Phys. **75**, 473 (2003).

[52] A. de la Torre, S. McKeown Walker, F. Y. Bruno, S. Riccó, Z. Wang, I. G. Lezama, G. Scheerer, G. Giriat, D. Jaccard, C. Berthod, T. K. Kim, M. Hoesch, E. C. Hunter, R. S. Perry, A. Tamai, and F. Baumberger, Phys. Rev. Lett. **115**, 176402 (2015).

[53] Y. K. Kim, O. Krupin, J. D. Denlinger, A. Bostwick, E. Rotenberg, Q. Zhao, J. F. Mitchell, J. W. Allen, and B. J. Kim, Science **345**, 187 (2014).